Large-Signal Stability Improvement of Parallel Grid-Forming Inverter-Driven Black Start

Preprint

Nathan Baeckeland and Gab-Su Seo

National Renewable Energy Laboratory

To be presented at the 2024 Conference on Innovative Smart Grid Technologies North America (ISGT NA)
Washington, D.C.
February 19–22, 2024

NREL is a national laboratory of the U.S. Department of Energy
Office of Energy Efficiency & Renewable Energy
Operated by the Alliance for Sustainable Energy, LLC

This report is available at no cost from the National Renewable Energy Laboratory (NREL) at www.nrel.gov/publications.

Contract No. DE-AC36-08GO28308

Conference Paper
NREL/CP-5D00-87250
November 2023

Large-Signal Stability Improvement of Parallel Grid-Forming Inverter-Driven Black Start

Preprint

Nathan Baeckeland and Gab-Su Seo

National Renewable Energy Laboratory

Suggested Citation
Baeckeland, Nathan, and Gab-Su Seo. 2023. *Large-Signal Stability Improvement of Parallel Grid-Forming Inverter-Driven Black Start: Preprint*. Golden, CO: National Renewable Energy Laboratory. NREL/CP-5D00-87250.
https://www.nrel.gov/docs/fy24osti/87250.pdf.

NREL is a national laboratory of the U.S. Department of Energy
Office of Energy Efficiency & Renewable Energy
Operated by the Alliance for Sustainable Energy, LLC

This report is available at no cost from the National Renewable Energy Laboratory (NREL) at www.nrel.gov/publications.

Contract No. DE-AC36-08GO28308

Conference Paper
NREL/CP-5D00-87250
November 2023

National Renewable Energy Laboratory
15013 Denver West Parkway
Golden, CO 80401
303-275-3000 • www.nrel.gov

NOTICE

This work was authored by the National Renewable Energy Laboratory, operated by Alliance for Sustainable Energy, LLC, for the U.S. Department of Energy (DOE) under Contract No. DE-AC36-08GO28308. This work was supported by the Laboratory Directed Research and Development Program at NREL and the U.S. Department of Energy's Office of Energy Efficiency and Renewable Energy (EERE) under the Solar Energy Technologies Office Award Number 38637. The views expressed herein do not necessarily represent the views of the DOE or the U.S. Government.

Cover Photos by Dennis Schroeder: (clockwise, left to right) NREL 51934, NREL 45897, NREL 42160, NREL 45891, NREL 48097, NREL 46526.

Large-Signal Stability Improvement of Parallel Grid-Forming Inverter-Driven Black Start

Nathan Baeckeland and Gab-Su Seo

Power Systems Engineering Center, National Renewable Energy Laboratory, Golden, CO 80401, USA
E-mails: {nathan.baeckeland, gabsu.seo}@nrel.gov

***Abstract*—With the rapid increase of inverter-based resources in modern grids, advanced grid-forming (GFM) inverter capabilities, such as system restoration and operation under faults, are urgently needed to realize power electronics-dominant grids at scale. One such capability is inverter-driven black start using GFM inverters. This paper analyzes the ability of two recently proposed advanced GFM controls to help GFM inverters sustain system-wide, off-nominal conditions and remain synchronized until they can overcome the momentary overloading as more GFMs join the process without generator sequence coordination or communications and finally stabilize the grid. Through an extensive set of 1,200 full-order electromagnetic transient simulations, we evaluate the black-start process while employing the various GFM inverter controls. The results show that the GFM current limiter and primary control have a significant impact on the stability of the system during dynamic operating conditions and thus impact the success of inverter-driven system restoration.**

***Index Terms*—Inverter-based black start, grid-forming inverter, large-signal stability, current limit, system restoration.**

I. Introduction

In a quickly changing power system, grid-forming (GFM) inverters are considered critical and cost-effective to take over certain responsibilities that are typically provided by synchronous generators compared to other technologies, such as synchronous condensers or new transmission lines [1], [2]. The U.S. Department of Energy, the Australian Energy Market Operator, the U.K. National Grid, and the European Network of Transmission System Operators for Electricity have all expressed urgency to incorporate GFM capabilities into inverter-based resources (IBRs) [3]–[6].

One GFM capability that has recently gained attention is using GFM inverters to black start and restore the grid. As GFM inverters can form a grid without synchronous generators, they can quickly bring a power system back into service, enhancing grid resilience and alleviating concerns about zero-inertia systems. Prior work has identified pathways to facilitate inverter-driven black start [7]. Other works have investigated the technical feasibility of a GFM inverter-driven black start in transmission systems [8], offshore wind power plants [9], and microgrid setups using multiple GFMs [10]. In particular, using multiple GFM IBRs for a black start in a decentralized manner would significantly increase the value position of GFM assets [11]. The parallel inverter black-start capability without leader-follower coordination would help improve grid resilience, increase the robustness of system restoration, and enhance flexible and cost-effective maintenance.

Although GFM controls allow IBRs to recover a large system, stringent inverter limits pose challenges to orchestrating a multiple GFM IBR black start and retaining stability during this off-nominal process. Incorporating a pre-synchronization block allows for the smooth interconnection of the GFM IBRs with the grid—passively [12] or actively; however, the post-synchronization stability is not guaranteed. During a black start, the system's baseline load can be too high for one GFM IBR to recover the grid voltage fully. A GFM inverter joining this overloaded system is immediately pushed into a prolonged current-limited operation until enough generation capacity is aggregated to cover the load [12]. GFM inverters operating in a current-limited mode of operation are prone to large-signal instability because they cannot maintain a constant voltage phasor, which can compromise the GFM controls [13], [14].

In this paper, we evaluate the robustness of GFM inverters against instability during black-start-induced overloading. We consider various GFM current-limiting control topologies and large-signal stabilizing methods that have been proposed in recent literature [14], [15]. Through extensive electromagnetic transient (EMT) simulations, this paper presents a performance analysis of GFM current-limiting controls during a black-start process. The remainder of this work is structured as follows: In Section II, we briefly examine why GFM inverters become unstable during current limiting. In Section III, we describe the simulation setup, including the network and GFM controls under consideration. We introduce the simulation cases and define metrics to assess large-signal stability. In Section IV, we assess stability from an extensive set of 1,200 full-order EMT simulations where 5 GFM inverters black start a 14-bus network. We provide our final remarks in Section V.

II. Challenges of IBR-Driven Black Start

GFM inverters employ a primary controller to generate a voltage and angle reference. As such, they share power without needing a phase-locked loop or communication links, as shown in Fig. 1. Droop control, virtual synchronous machine (VSM) control, and dispatchable virtual oscillator control (dVOC) are some examples of primary controllers. This work uses the

This work was authored by the National Renewable Energy Laboratory (NREL), operated by Alliance for Sustainable Energy, LLC, for the U.S. Department of Energy (DOE) under Contract No. DE-AC36-08GO28308. This work was supported by the Laboratory Directed Research and Development Program at NREL and the U.S. Department of Energy's Office of Energy Efficiency and Renewable Energy (EERE) under the Solar Energy Technologies Office Award Number 38637.

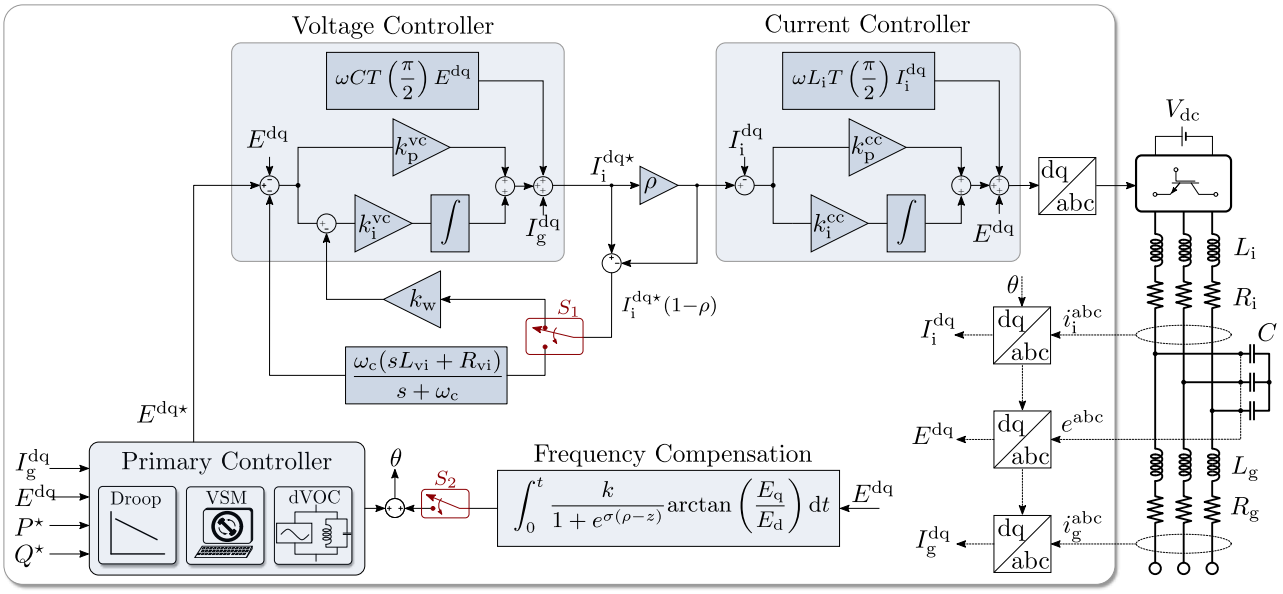

Fig. 1: GFM control system under consideration. Switches S_1 and S_2 allow for modifying the controls and enabling certain control blocks.

droop primary controller; more details on the GFM controls can be found in Section III. The following droop equations govern the reference voltage and angle of the inverter:

$$\frac{\mathrm{d}\theta}{\mathrm{d}t} = \omega^{\star}_{\mathrm{gfm}} = \omega_0 + m_{\mathrm{p}}(P^{\star} - P), \tag{1}$$

$$E^{\star} = E_0 + m_{\mathrm{q}}(Q^{\star} - Q), \tag{2}$$

where θ, $\omega^{\star}_{\mathrm{gfm}}$, and $E^{\star}$ denote the GFM reference angle, frequency, and voltage, respectively; and ω_0 and E_0 are the nominal values for frequency and voltage, respectively. The P-f and Q-V droop gains are denoted by m_{p} and m_{q}, respectively; and P, Q, $P^{\star}$, and $Q^{\star}$ denote the low pass-filtered output power and power set points, respectively.

An inverter during black start can be pushed into overloading for various reasons, including transformer or motor load inrush currents, insufficient load shedding, or a baseline load greater than the single inverter rating in a collective black start. To avoid damage to the power electronics inverter hardware, the control system curtails the inverter output current to acceptable predetermined values, typically from approximately 1.05 pu to 1.20 pu; however, this has significant ramifications on the behavior of the inverter during overcurrent. When in a current-limited state, the GFM inverter cannot match its output power, P, to reach a stable equilibrium in (1); for more discussion, see [14]. This can lead to an increasing internal GFM reference frequency, $\omega^{\star}_{\mathrm{gfm}}$, according to (1). If the current-limited state prolongs for too long, the internal reference angle, θ, can drift into an unstable operating point. In a GFM inverter-driven grid with multiple inverters pushed into unstable operating conditions, this can lead to system-wide instability where parts of the network lose synchronism with each other. Prolonged overloading can occur during an inverter-driven black start for large power systems involving multiple GFMs in a decentralized manner; thus, this paper investigates the robustness of various GFM inverter controls against large-signal instability.

III. Simulation Setup

This section first discusses the grid and inverter control topologies under consideration. We define the simulation cases for the black-start simulations. Lastly, we define metrics that allow us to assess the network stability during the black start.

A. Grid and Inverter Topology

To assess GFM inverter stability during a black start, we consider the modified IEEE 14-bus network, shown in Fig. 2, where five GFM inverters (1 pu each) and three resistive loads (4 pu in total) are interconnected. This work does not model transformers, line capacitance, motor loads, or constant power loads for computation burden and simplicity; more details of their impact can be found in [10], [11]. The line admittances are listed in Table I. Each inverter is equipped with a breaker to facilitate a grid interface. Fig. 1 shows the GFM control structure under study: cascaded voltage and current controllers in the synchronous reference frame. The primary controller governs the internal reference angle and voltage that are fed to the voltage loop. The inverter parameters are listed in Table II.

As illustrated in Fig. 1, the control system can be modified through switches S_1 and S_2. The switch S_1 activates the chosen current limiter. In this paper, we consider two current-limiting methods: (i) the current-reference saturation limiter (SatLim) and (ii) the hybrid limiter that combines the current-reference saturation and virtual impedance limiting methods (hybrid) [15]. The SatLim curtails the current references (denoted by ρ in Fig. 1), while an anti-windup feedback loop avoids integrator windup in the voltage controllers during current limiting. The hybrid limiter does the same; however, the output current angle is manipulated through the virtual impedance in the voltage feedback loop. As a result, the hybrid limiter combines the benefit of both SatLim and regular virtual impedance limiting, fully using the overcurrent capability of the inverter. More details can be found in [15]. The second switch, S_2, activates an additional frequency compensation

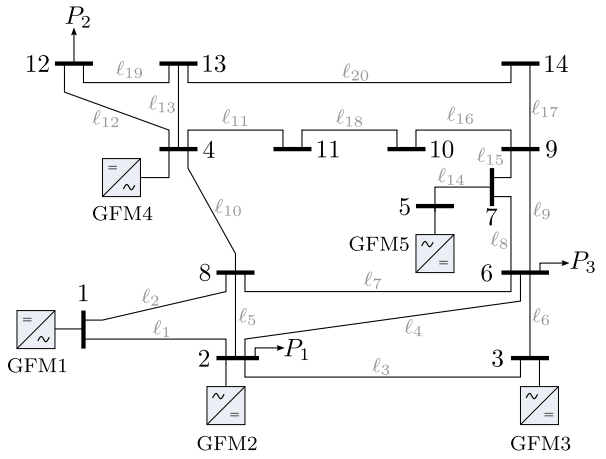

Fig. 2: Modified IEEE 14-bus network with five GFM inverters and three resistive loads interconnected.

TABLE I: Line-admittance magnitudes in pu, With θ_{line}=75°.

Line	ℓ_1	ℓ_2	ℓ_3	ℓ_4	ℓ_5	ℓ_6	ℓ_7	ℓ_8	ℓ_9	ℓ_{10}
$\lvert Y_{\text{line}}\rvert$	6.39	1.69	1.91	2.14	2.17	2.21	8.96	1.80	0.68	1.50
Line	ℓ_{11}	ℓ_{12}	ℓ_{13}	ℓ_{14}	ℓ_{15}	ℓ_{16}	ℓ_{17}	ℓ_{18}	ℓ_{19}	ℓ_{20}
$\lvert Y_{\text{line}}\rvert$	1.90	1.48	2.90	2.14	3.43	4.47	1.40	1.96	1.89	1.08

block. This method was proposed in [14] to enhance the large-signal stability of GFM inverters during faults and nonideal conditions.

Finally, each GFM inverter has a pre-synchronization block for smooth grid connection (not shown in Fig. 1) [12]. The pre-synchronization in this study ensures that the internal reference angle equals the grid voltage angle at the time of breaker closing to minimize the inrush currents. On the other hand, when no grid voltage is available or the voltage is not sizably established yet (less concern for forceful synchronization), e.g., $V_{\text{grid}} < 0.15\,\text{pu}$, i.e., for the case of the first GFM to initiate the black-start process from zero voltage, the pre-synchronization can be bypassed.

B. Simulation Cases

By changing the settings of switches S_1 and S_2 in Fig. 1, we study four different simulation cases:

TABLE II: Inverter and network parameters (all GFMs are identical).

Parameter	Value	Unit	Parameter	Value	Unit
ω_{s}	$2\pi 60$	$\text{rad}\cdot\text{s}^{-1}$	k_{p}^{cc}	0.9817	pu
θ_ℓ	75	°	k_{i}^{cc}	0.0018	pu
$L_{\text{i}}\omega_{\text{s}}$	0.0196	pu	ω_{i}	$2\pi 3000$	$\text{rad}\cdot\text{s}^{-1}$
R_{i}	0.0139	pu	ω_{v}	$2\pi 500$	$\text{rad}\cdot\text{s}^{-1}$
$C\omega_{\text{s}}$	0.1086	pu	k_{p}^{vc}	1.4476	pu
$L_{\text{g}}\omega_{\text{s}}$	0.0196	pu	k_{i}^{vc}	0.0273	pu
R_{g}	0.0139	pu	$I_{\max}$	1.2	pu
m_{p}	2	%	m_{q}	5	%

ω_{s}: nominal angular grid frequency, θ_ℓ: line impedance angle, L_{i}, R_{i}, C, L_{g}, and R_{g}: the LCL output filter parameters, k_{p}^{cc}, k_{i}^{cc}, k_{p}^{vc}, and k_{i}^{vc}: inverter proportional and integral control gains for the inner-current and outer-voltage loops, ω_{i} and ω_{v}: inner-current and outer-voltage loop bandwidths. m_{p}, m_{q}: the $P-f$ and $Q-V$ droop gains.

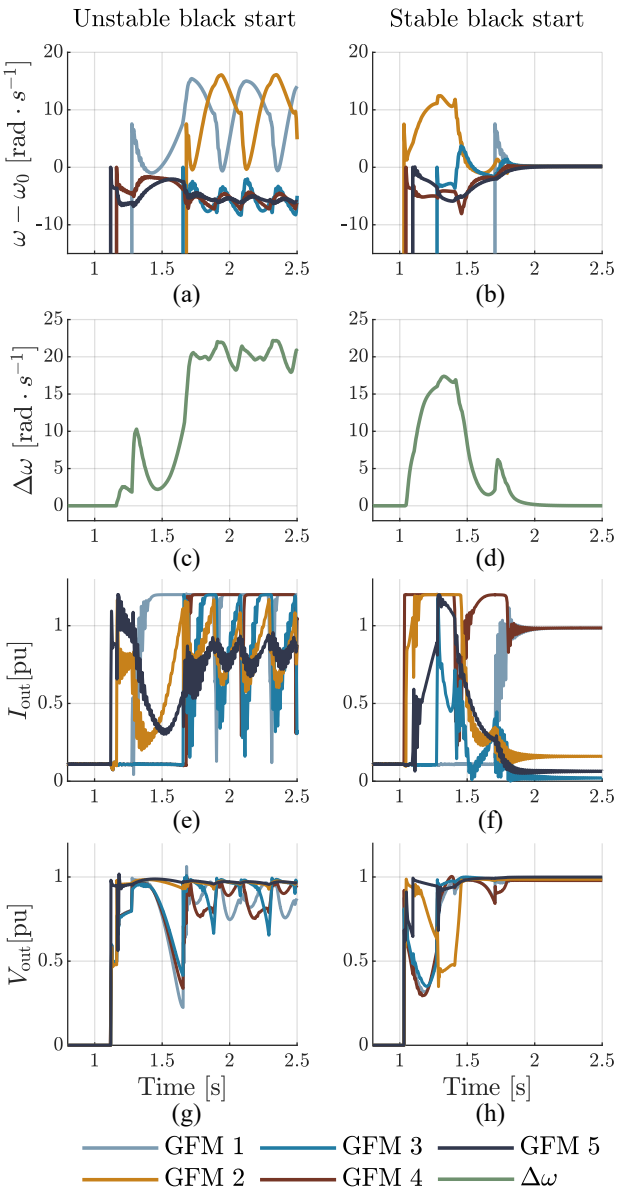

Fig. 3: Black-start cases, unstable (left) and stable (right): (a)–(b) inverter reference frequencies, (c)–(d) difference between highest and lowest GFM frequencies ($\Delta\omega$), (e)–(f) currents, and (g)–(h) voltages.

Case #1: SatLim without frequency compensation
Case #2: Hybrid limiting without frequency compensation
Case #3: SatLim with frequency compensation
Case #4: Hybrid limiting with frequency compensation.

For each of the four GFM control topologies, we simulate a random black-start sequence to emulate the autonomous black start, driven by multiple GFM IBRs without communication. For this, we randomly create five timestamps at which we close the inverter breakers. To obtain a representative set of simulations from which to draw conclusions, we run 100 randomized scenarios with different breaker closing times per case, yielding 400 simulation results. In addition, to evaluate the impact of the breaker closing window, i.e., to study how the responsiveness and turn-on interval of the black-starting GFM inverters affects the success of the black start, we have three sets of breaker closing time windows: 1 s, 3 s, and 10 s. We

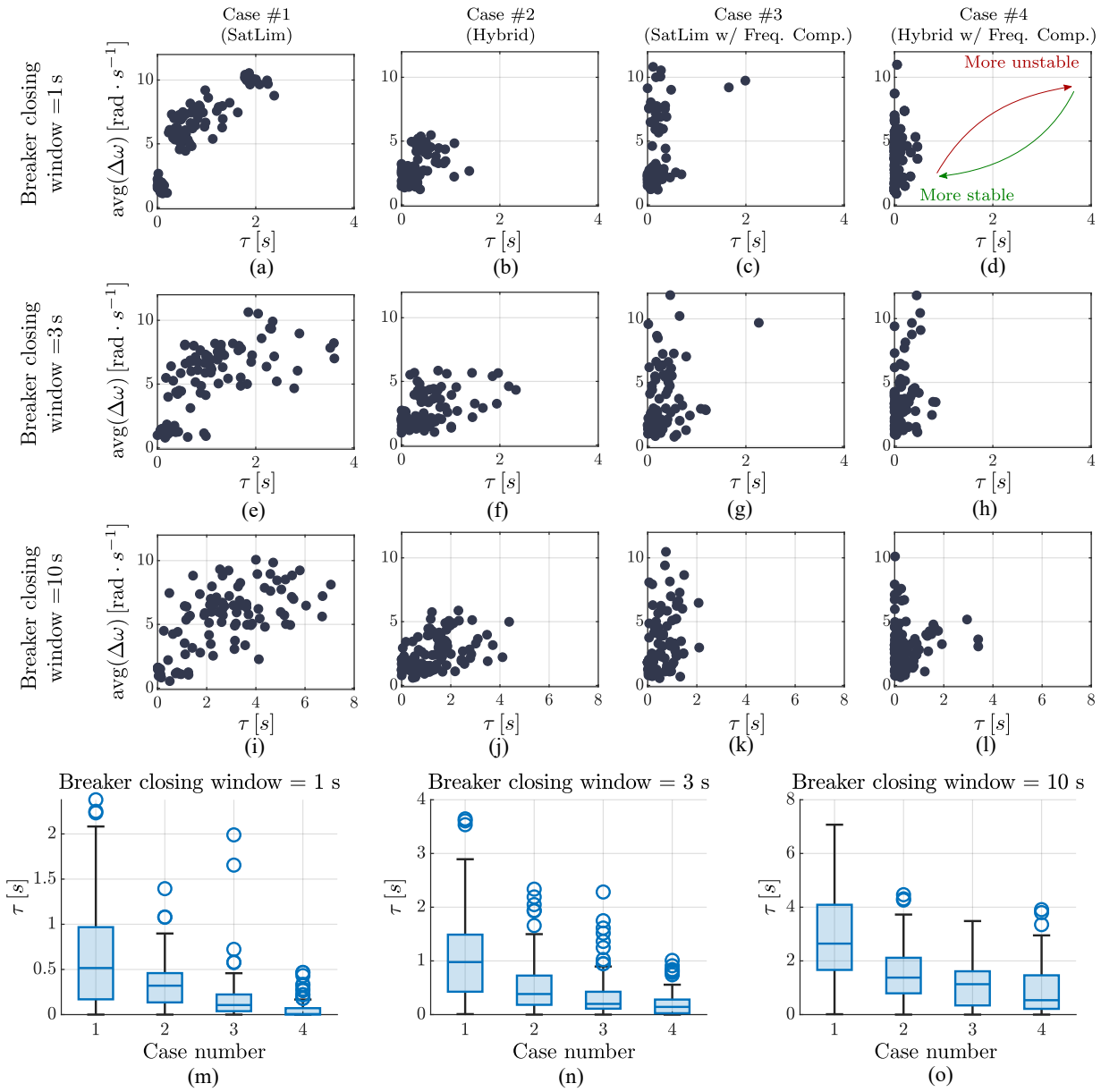

Fig. 4: Results of the 1,200 EMT simulation runs: (a)–(d), (e)–(h), and (i)–(l) show scatter plots of the duration of instability (τ, x-axis) and $\text{avg}(\Delta\omega)$ (y-axis) of each simulation run for the four cases with a breaker closing window of 1 s, 3 s, and 10 s, respectively, (m)–(o) show box plots for each case and breaker closing window, respectively. Definitions of the stability metrics are in Section III-C.

randomly generate 100 breaker closing times within each time span (1 s, 3 s, or 10 s) that is used for all four simulation cases. In other words, all the breakers are guaranteed to be closed within the time span. Apart from the current-limiting controls and the breaker timing, all simulations are homogeneous.

C. Large-Signal Stability Performance Metrics

In this subsection, we define two performance metrics to assess the influence of the four GFM topologies on the network stability during an inverter-driven black start. In this work, we consider the grid in Fig. 2 as stable if all the inverters are synchronized, i.e., their reference frequencies from the primary controller settle at the same value. For the computation, we first introduce $\Delta\omega = \Omega_{\max} - \Omega_{\min}$, where Ω is the array of the inverter frequencies. Taking the derivative of $\Delta\omega$ gives information about whether the grid is converging to synchronism (moving toward stability) or diverging (instability). We denote the total time of the diverging frequencies by $\tau = \int f(t)\mathrm{d}t$, where $f(t)$ is 1 when $\frac{\mathrm{d}}{\mathrm{d}t}(\Delta\omega(t)) > 0$, or 0 otherwise; thus, the smaller τ is, the less time the grid is in unstable operation during or after the black-start process. We use τ as a metric to assess and compare the duration of instability of the cases during the black-start process. The second metric is the average of $\Delta\omega$ over the duration of the black start, which we define as the time between when the second inverter comes online and when all five inverters are online with matching frequencies (the grid is fully restored and stable). We denote this metric by $\text{avg}(\Delta\omega)$. Accordingly, this metric represents the degree of frequency mismatch among GFM IBRs during the black start. The higher $\text{avg}(\Delta\omega)$, the further away the grid is from synchronization where all the inverter frequencies are matched. Note that these metrics allow for comparing cases

in terms of stability, without classifying them as either stable or unstable.

Fig. 3 illustrates an unstable (left column) and a stable (right column) black-start case, which are randomly chosen from the batch of 100 simulation runs from Case #1 with a breaker closing window of 1 s. Figs. 3(a)–(b) show the internal GFM frequencies of all five inverters that are randomly coming online during the black start. Figs. 3(c)–(d) show the corresponding $\Delta\omega$, which is zero when there are less than two inverters active in the grid or if the grid-connected inverters are synchronized. The output currents, shown in Figs.3(e)–(f), illustrate that some inverters are hitting the current limit (1.2 pu) during the black start.

IV. Simulation Results and Discussion

The results of all 1,200 EMT simulation runs are visualized in Fig. 4. In the scatter plots in Fig. 4(a)–(l), every dot represents one black-start simulation run. The horizontal axis denotes τ, i.e., duration of instability, and the vertical axis denotes $\mathrm{avg}(\Delta\omega)$. Without quantifying stability, the scatter plots provide a visual tool to compare and assess which case yields a more stable black start. The more the dots are located near the origin, i.e., in the bottom left corner, the more stable the black start is (mildly unsynchronized, and quickly reaching synchronism). On the other hand, the more dots are in the top right corner, the more unstable the black start is (highly unsynchronized, and a long recovery to synchronism).

From the scatter plots, observations and discussions on the black-start stability follow. For all the considered breaker time windows (1 s, 3 s, and 10 s), the hybrid limiter (Case #2) shown in Figs. 4(b), 4(f), and 4(j) shows superior black-start stability compared to the SatLim (Case #1) in Figs. 4(a), 4(e), and 4(i), respectively. Second, adding the synchronization term decreases the duration of the black-start-induced instability, τ, significantly, as illustrated by both Case #3 and #4. At the same time, adding the synchronization term increases $\mathrm{avg}(\Delta\omega)$, especially for Hybrid (Case#4). The additional term leads the GFM internal angles to synchronize faster, resulting in smaller τ, as shown in the results of Case #3 and #4. On the other hand, note that the term may result in greater $\mathrm{avg}(\Delta\omega)$ values in some cases, as shown in Fig. 4. For instance, since the time of the averaging $\mathrm{avg}(\Delta\omega)$ is significantly shorter with the synchronization term, the metric could be computed greater in cases of higher presynchronization frequency mismatch in which its impact may more pronounce. Further study on the impact of the term is in progress.

In Fig. 4(m)–(o), the box charts are shown for all cases with different breaker time windows, which provide another tool to compare τ. The box charts convey that Case #4 yields faster synchronization during the black start than Case #3. Similarly, Case #2 performs better in terms of τ than Case #1; hence, with or without the additional synchronization term, the hybrid limiter yields a more stable black start than the SatLim. Overall, Case #4—where we leverage the hybrid limiter and the synchronization term—yields superior black starts compared to the other cases. These results illustrate that GFM inverter manufacturers and other stakeholders should be mindful that a pre-synchronization logic does not guarantee a stable synchronization of the inverter with the grid. Yet, additional design considerations would be instrumental for a reliable IBR-driven black start.

V. Conclusion

During an inverter-driven black start for a large power system, the GFM IBRs can be pushed into overloading during which they are prone to losing synchronism, thus causing system-wide instability. This work has analyzed the ability of different GFM inverter controls to achieve a stable black start without leader-follower coordination or communications. Through an extensive set of 1,200 full-order EMT simulations, we have evaluated the effect of two different current limiters and a synchronization method on the overloaded inverter-driven black start. The results confirm that pre-synchronization does not suffice for a stable black start. Namely, how the GFM control handles the overloading affects the success of the black start. We found that employing the hybrid current limiter—which combines concepts of current-reference saturation and virtual impedance limiting—in combination with a frequency synchronization method greatly improves system stability during a GFM inverter-driven black start.

References

[1] Y. Lin *et al.*, "Research roadmap on grid-forming inverters," National Renewable Energy Lab.(NREL), Golden, CO (U.S.), Tech. Rep., 2020.

[2] "Transition to fewer synchronous generators in south australia-transition to fewer synchronous generators in south australia," Australian Energy Market Operator (AEMO), Tech. Rep., 2023.

[3] D. Ramasubramanian et al., "Performance specifications for grid-forming technologies," in *Proc. IEEE Power & Energy Soc. Gen. Meet.*, 2023, pp. 1–6.

[4] AEMO, "Application of advanced grid-scale inverters in the nem," 2021.

[5] National Grid ESO, "Draft Grid Code – Grid Forming Converter Specification 3 rd September 2020," Tech. Rep. September, 2020.

[6] ENTSO-e, "High Penetration of Power Electronic Interfaced Power Sources and the Potential Contribution of Grid Forming Converters Technical Report," Tech. Rep., 2020.

[7] H. Jain, G.-S. Seo, E. Lockhart, V. Gevorgian, and B. Kroposki, "Blackstart of power grids with inverter-based resources," in *IEEE Power & Energy Society General Meeting*, 2020, pp. 1–5.

[8] L. Noris, J. Rueda, E. Rakhshani, and A. Korai, "Power system black-start and restoration with high share of power-electronic converters," in *IEEE Power & Energy Soc. Gen. Meet.*, 2019, pp. 1–5.

[9] A. Jain, J. N. Sakamuri, and N. A. Cutululis, "Grid-forming control strategies for black start by offshore wind power plants," *Wind Energy Science*, vol. 5, no. 4, pp. 1297–1313, 2020.

[10] J. Sawant, G.-S. Seo, and F. Ding, "Resilient inverter-driven black start with collective parallel grid-forming operation," in *Proc. IEEE Innovative Smart Grid Technol. Conf.*, 2023, pp. 1–5.

[11] G.-S. Seo, J. Sawant, and F. Ding, "Black start of unbalanced microgrids harmonizing single- and three-phase grid-forming inverters," in *IEEE Power & Energy Society General Meet.*, 2023, pp. 1–6.

[12] H. Chang, N. Baeckeland, A. Banerjee, and G.-S. Seo, "Universal passive synchronization method for grid-forming inverters without mode transition," in *Proc. Int. Conf. Power Electron.*, 2023, pp. 1523–1529.

[13] L. Huang, L. Zhang, H. Xin, Z. Wang, and D. Gan, "Current limiting leads to virtual power angle synchronous instability of droop-controlled converters," in *IEEE Power & Energy Soc. Gen. Meet.*, 2016, pp. 1–5.

[14] N. Baeckeland and G.-S. Seo, "Frequency synchronization of grid-forming inverters under fault conditions and overloading," in *IEEE Workshop on Control and Modelling of Power Electron.*, 2023, pp. 1–8.

[15] ——, "Novel hybrid current limiter for grid-forming inverter control during unbalanced faults," in *Proc. Int. Conf. Power Electron.-ECCE Asia*, 2023, pp. 1517–1522.